Rapid and facile ratiometric detection of an anthrax biomarker by regulating energy transfer process in bio-metal–organic…

Article *in* Biosensors & Bioelectronics · May 2016

DOI: 10.1016/j.bios.2016.05.020

CITATIONS
3

READS
36

5 authors, including:

Ma Heping
Changchun Institute of Optics, Fine Mechanics and Physics
28 PUBLICATIONS **504** CITATIONS

SEE PROFILE

Contents lists available at ScienceDirect

Biosensors and Bioelectronics

journal homepage: www.elsevier.com/locate/bios

Rapid and facile ratiometric detection of an *anthrax* biomarker by regulating energy transfer process in bio-metal-organic framework

Yihe Zhang [a,b], Bin Li [a,*], Heping Ma [a,*], Liming Zhang [a], Youxuan Zheng [a,c]

[a] State Key Laboratory of Luminescence and Applications, Changchun Institute of Optics Fine Mechanics and Physics, Chinese Academy of Sciences, Changchun 130033, PR China
[b] University of Chinese Academy of Sciences, Beijing 100039, PR China
[c] State Key Labortory of Coordination Chemistry, Nanjing National Laboratory of Microstructures, School of Chemistry and Chemical Engineering, Nanjing University, Nanjing 210093, PR China

ARTICLE INFO

Article history:
Received 2 March 2016
Received in revised form
25 April 2016
Accepted 3 May 2016
Available online 7 May 2016

Keywords:
Metal-organic frameworks
Lanthanide
Energy transfer
Colorimetric sensor
Dipicolinate acid

ABSTRACT

A ratiometric fluorescent sensor based on luminescent bio-metal-organic framework was prepared by exchanging both Tb^{3+} and Eu^{3+} cations into anionic bio-MOF-1. Due to a highly efficient energy transfer from Tb^{3+} to Eu^{3+} (> 89%), emission color of Tb/Eu@bio-MOF-1 was orange-red even though Tb^{3+} was the dominant content in this Tb/Eu co-doping material. More interestingly, this energy transfer process could be modulated by dipicolinic acid (DPA), an unique biomarker for bacillus spores. With DPA addition, corresponding DPA-to-Tb^{3+} energy transfer was gradually enhanced while the energy transfer from Tb^{3+} to Eu^{3+} was significantly weakened. By regulating the energy transfer process in Tb/Eu@bio-MOF-1, visual colorimetric sensing of DPA in porous MOF was realized for the first time. Detection limit of Tb/Eu@bio-MOF-1 for DPA was 34 nM, which was much lower than an infectious dosage of *Bacillus anthracis* spores (60 μM) for human being. Besides, Tb/Eu@bio-MOF-1 showed a remarkable selectivity over other aromatic ligands and amino acids. More importantly, this porous ratiometric sensor worked equally well in human serum. These particularly attractive features of Tb/Eu@bio-MOF-1 made the direct, rapid and naked-eye detection of DPA for practical application possible.

1. Introduction

Anthrax is one of the acute infectious disease which infects both animals and humans. *Bacillus anthracis* has been reported as a potential bioterrorism agent since the *anthrax* attack in the U. S. in 2001, and still attracts broad attention throughout the world (Webb, 2003; Yung et al., 2007). A number of attempts have been made to detect bacillus spores such as bacteriology, serology-immunoassays and polymerase chain reactions (PCR) (Das et al., 2015; Hurtle et al., 2004). However, traditional biological methods usually require lengthy cycles, complicated operation, expensive reagents and professional analysis, making them not suitable for on-line monitoring (Su et al., 2016). Rapid, sensitive and straightforward detection of bacillus spores is crucial for disease and bioterrorism prevention (Ai et al., 2009). Recently, optical techniques for dipicolinic acid (DPA, a unique biomarker and major constituent of bacterial spores) detection have caused wide concern due to their low cost, fast response and easy portability. Surface enhanced Raman spectroscopy (SERS) and surface plasmon resonance (SPR) biosensors have been explored to detect biological molecules, respectively (Gao et al., 2015; Lepage et al., 2013; Zhang et al., 2005). Another convenient optical sensing technique for biological molecules is based on lanthanide luminescence method, which is rapid, selective and highly sensitive (Oh et al., 2011; Yilmaz et al., 2010). In previous reports, terbium (Tb) has been proved effective for DPA detection (Rosen et al., 1997; Tsukube and Shinoda, 2002). However, its nonselective binding for anionic interferents limits its further application. Europium (Eu) based nanocomposite has shown improved selectivity (Ai et al., 2009). However, Tb-based and Eu-based sensors determine DPA concentration through emission intensity variation which is greatly influenced by excitation, environmental and instrumental factors (Li et al., 2013). Sensing reliability can be improved by using a ratiometric fluorescent sensor, which measures the ratio between analyte signal and reference signal (Guan et al., 2015; Zou et al., 2014).

Luminescence from lanthanide ions is usually weak due to their forbidden f-f transitions. Many proposals have been reported to enhance their luminescence such as coordinating to organic ligands or being doped into special matrices (Eliseeva and Bunzli, 2010; Shen and Yan, 2015a; Zhang et al., 2015). There are several advantages in introducing lanthanide centers into metal organic

* Corresponding authors.
E-mail addresses: libinteacher@163.com (B. Li), mahp@ciomp.ac.cn (H. Ma).

http://dx.doi.org/10.1016/j.bios.2016.05.020
0956-5663/

frameworks (Chen et al., 2010; White et al., 2009). Firstly, MOFs have a number of photons emitted in per unit volume, which enhances lanthanide luminescence (An et al., 2011). Secondly, their excellent stability and porous rigid scaffold protect lanthanide ions from complex environment. Thirdly, their high adsorption volume and large surface area can gather analyte and amplify reaction zone (Wang et al., 2012). Most importantly, MOFs structures can be precisely designed and manipulated to meet specific needs.

Herein, we present a direct and rapid strategy for colorimetric detection of *Bacillus anthracis* biomarker DPA using Tb^{3+}/Eu^{3+} co-doped Bio-MOF (here-after denoted as Tb/Eu@bio-MOF-1). Luminescent Tb/Eu@bio-MOF-1 was synthesized via exchanging Tb^{3+} and Eu^{3+} cations into anionic bio-MOF-1. The resulting MOF exhibited orange-red emission color due to a highly efficient energy transfer from Tb^{3+} to Eu^{3+}. After meeting DPA, DPA-to-Tb^{3+} energy transfer was gradually enhanced while the energy transfer from Tb^{3+} to Eu^{3+} was significantly weakened, leading to fluorescence color change from orange-red to green. For the first time, we realized visual colorimetric sensing of DPA by regulating the energy transfer process in Tb/Eu@bio-MOF-1.

2. Materials and methods

2.1. Chemicals and materials

Adenine, 4,4′-biphenyl dicarboxylic acid (BPDC), zinc acetate dihydrate, 2,6-pyridinedicarboxylic acid (DPA) were purchased from commercial sources. $Eu(NO_3)_3$●6 h_2O was obtained by dissolving Eu_2O_3 in concentrated nitric acid with agitation, and then heating this solution to dryness. In addition to adding hydrogen peroxide, $Tb(NO_3)_3$●6 h_2O was obtained by the same way from Tb_4O_7. Unless otherwise mentioned, all purchased analytical grade solvents were used without further purifications. Double distilled water was used in this work.

2.2. Characterization

X-ray powder diffraction (XRD) patterns were obtained from a Bruker D4 X-ray diffractometer (Germany) with Cu $K\alpha_1$ radiation (λ=1.5405 Å, 40 kV, 30 mA). Scanning electron microscopy (SEM) images were measured on a Hitachi S-4800 microscope. Contents of Tb^{3+}, Eu^{3+} and Zn^{2+} in our work were determined by an iCAP6300 inductively coupled plasma-optical emission spectrometer (ICP-OES, US Thermo Scientific). Samples were prepared by decomposing the powder samples into concentrated nitric acid, followed by ultrasonic treatment and dilution to 1% nitric acid solution. N_2 adsorption and desorption isotherms were measured at liquid nitrogen temperature, using a Nova l000 analyzer (US Quantachrome Corporation Company). Samples were degassed in vacuum at 150 °C for at least 10 h before adsorption and their surface area values were calculated according to Brunauer-Emmett-Teller (BET) equation. Fluorescence excitation and emission spectra were recorded on a Hitachi F-7000 fluorescence spectrophotometer using a 450 W xenon lamp as excitation source. Emission lifetimes were measured with a Lecroy Wave Runner 6100 Digital Oscilloscope (1 GHz) using a tunable laser as excitation source (Continuum Sunlite OPO) and calculated by exponential fitting.

2.3. Preparation of bio-MOF-1

Construction route for Tb/Eu@bio-MOF-1 sensor and DPA sensing mechanism are depicted in Scheme 1. Bio-MOF-1 was synthesized through a solvothermal method as reported previously (An et al., 2009). Typically, adenine (0.25 mmol), 4,4′-biphenyl dicarboxylic acid (0.5 mmol) and zinc acetate dihydrate (0.75 mmol) were dissolved in DMF (27 mL) and water (2 mL) and stirred vigorously for 60 min, then nitric acid (2 mmol) was added. After these reagents were well mixed, this mixture was sealed in a 40 mL Teflon-lined stainless-steel autoclave, heated at 130 °C for 48 h. Rod-shaped crystals were collected and washed with DMF and dichloromethane (CH_2Cl_2) several times and dried in vacuum at 60 °C overnight.

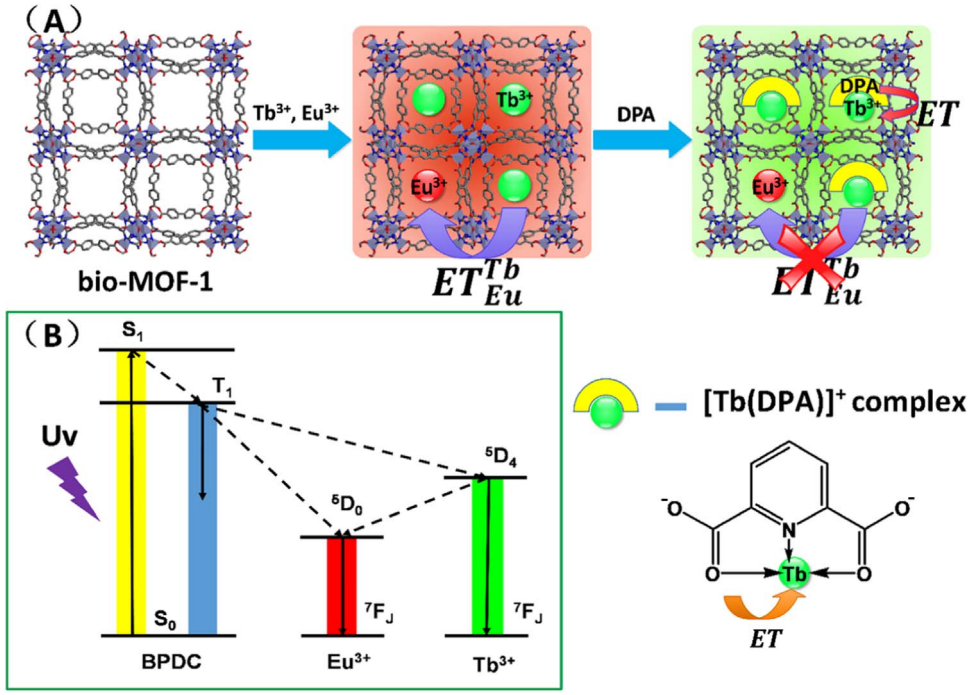

Scheme 1. (A) Synthesis strategy of Tb/Eu@bio-MOF-1 and its principle for the detection of DPA; (B) Schematic diagram of the ligand-metal energy transfer from triplet state of the BPDC to Ln^{3+} ions and the metal-metal energy transfer from $^5D_4$ of the Tb^{3+} to $^5D_0$ of the Eu^{3+} ions.

2.4. Post-synthetic cation exchange of bio-MOF-1 with Tb^{3+}, Eu^{3+}

Ln@bio-MOF-1 (Ln=Tb^{3+}, Eu^{3+}) samples were performed by replaced dimethylammonium cations (DMA^{+}) in bio-MOF-1 with Ln^{3+} ions via cation exchange (An et al., 2011; Li et al., 2014). In a typical process, as-synthesized bio-MOF-1 was soaked in DMF solution of $Tb(NO_3)_3 \bullet 6H_2O$ (0.1 M) at 65 °C for 30 min; after 3 times later, the material was again soaked in the DMF solution of $Tb(NO_3)_3 \bullet 6H_2O$ (0.1 M), repeated every 24 h for 3 days. Then the products were thoroughly washed with ethanol and dried in vacuum at 100 °C for 24 h. The exchange of Tb/Eu@bio-MOF-1 was performed using the same procedure, except that corresponding bimetallic material was soaked in the specified ratio of mixed Ln^{3+} nitrates (Tb^{3+}/Eu^{3+} =3, 6 and 10, respectively).

2.5. Preparation of the Ln@bio-MOF-1 films

All Ln@bio-MOF-1 films were prepared by a direct spin-coating method onto a pre-cleaned glass-substrate. Typically, a thin layer of photoresist was dripped onto a 2 cm × 2 cm glass substrate using a Laurell spin-coater to form an adhesion phase. Then suspension with 10–15 mg/mL Ln@bio-MOF-1 was dripped onto this photoresist layer with spin rate of 2000 rpm for 60 s. This spun process was repeated several times until film surface was smooth and continuous. Adsorbed solvent was removed in the air.

2.6. Detection of DPA

In a typical run, Tb/Eu@bio-MOF-1 was dispersed with a final concentration of 0.25 mg/mL in aqueous solution, luminescence measurement was taken 20 s later after analyte was injected. To evaluate this biosensor for practical analysis, human serum samples were spiked with standard DPA solutions and then analyzed with Tb/Eu@bio-MOF-1 solution. The excitation spectra are measured by monitoring the characteristic emission wavelengths at 545 nm for Tb^{3+} and 615 nm for Eu^{3+}, respectively. Samples were excited at 290 nm with excitation and emission wavelength band passes both set as 5 nm.

3. Results and discussion

3.1. Phase formation and structural characters

XRD diffraction patterns of bio-MOF-1 and Ln@bio-MOF-1 (Ln=Tb^{3+}, Eu^{3+}) are shown in Fig. 1(A). Diffraction peaks of bio-MOF-1 are well conformed to those of literature reports (An et al., 2009; An et al., 2011). No peaks from impurities are detected in Ln@bio-MOF-1 after ion exchange, which implies that the incorporation of lanthanide ions in pore does not impact bio-MOF-1 crystal structure. Ln@bio-MOF-1 morphology is not changed as confirmed by SEM images (Fig. S1 in supplementary material). Tb^{3+} and Eu^{3+} content ratio in Tb/Eu@bio-MOF-1 is determined by an inductive coupled plasma (ICP)-optical emission spectrometer. According to this ICP result, Tb^{3+} content is higher than Eu^{3+} content and the content ratio of Tb^{3+}:Eu^{3+} content ratio is basically consistent with their initial concentration ratio (Table S1 in Supplementary Material). Fluorescence microscopy images of as-synthesized bio-MOF-1 and Ln@bio-MOF-1 are shown in Fig. S2. Bio-MOF-1 exhibits blue emission, which derives from BPDC linkers. After lanthanide cations are incorporated into this pore matrix, single-ion-doped composites display their characteristic luminescence emission in green region for Tb@bio-MOF-1 and red region for Eu@bio-MOF-1, respectively. While in the co-doped composite with Tb^{3+}/Eu^{3+} of 6:1, orange-red emission is observed even though Tb^{3+} is the dominant content ion. Corresponding color changes can be explained by energy transfer process (Li et al., 2010; Yu et al., 2015; Zhao et al., 2015), which will be discussed later.

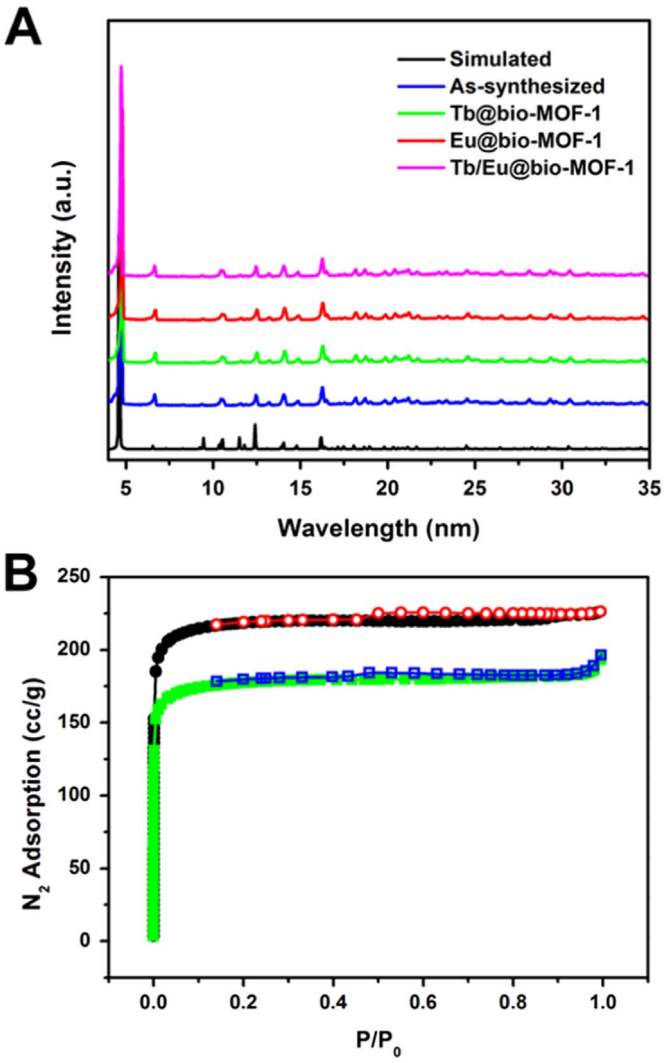

Fig. 1. (A) X-ray powder diffraction patterns of bio-MOF-1 (black, simulated; blue, as-synthesized; green, Tb@bio-MOF-1; red, Eu@bio-MOF-1; amaranth, Tb/Eu@bio-MOF-1). (B) Nitrogen adsorption-desorption isotherms for bio-MOF-1 (black filled, adsorption; red empty, desorption) and Tb/Eu@bio-MOF-1 (green filled, adsorption; blue empty, desorption). (For interpretation of the references to color in this figure legend, the reader is referred to the web version of this article.)

Nitrogen adsorption isotherms of as-synthesized bio-MOF-1 and Tb/Eu@bio-MOF-1 are collected and demonstrated in Fig. 1(B). These curves match characteristic type-I isotherms very well, which illustrates their successful synthesis (microporous bio-MOF-1). BET surface area for bio-MOF-1 and Tb/Eu@bio-MOF-1 are 943.38 $m^2\ g^{-1}$ and 765.10 $m^2\ g^{-1}$, respectively. The less N_2 uptake capacity for Tb/Eu@bio-MOF-1 than that of bio-MOF-1 is caused by the incorporation of Tb^{3+} and Eu^{3+} cations in MOF pore.

3.2. Luminescent properties

Excitation and emission spectra of Ln@bio-MOF-1 in aqueous solutions are presented in Fig. 2. These spectra show similar excitation bands ranging in 230–400 nm with a maximum peak at around 290 nm, which greatly matches for BPDC absorption. This result indicated that the trivalent rare earth ions are sensitized by BPDC in bio-MOF-1 effectively (Shen and Yan, 2015b; Zou et al., 2014). Tb@bio-MOF-1 exhibits Tb^{3+} characteristic transitions at

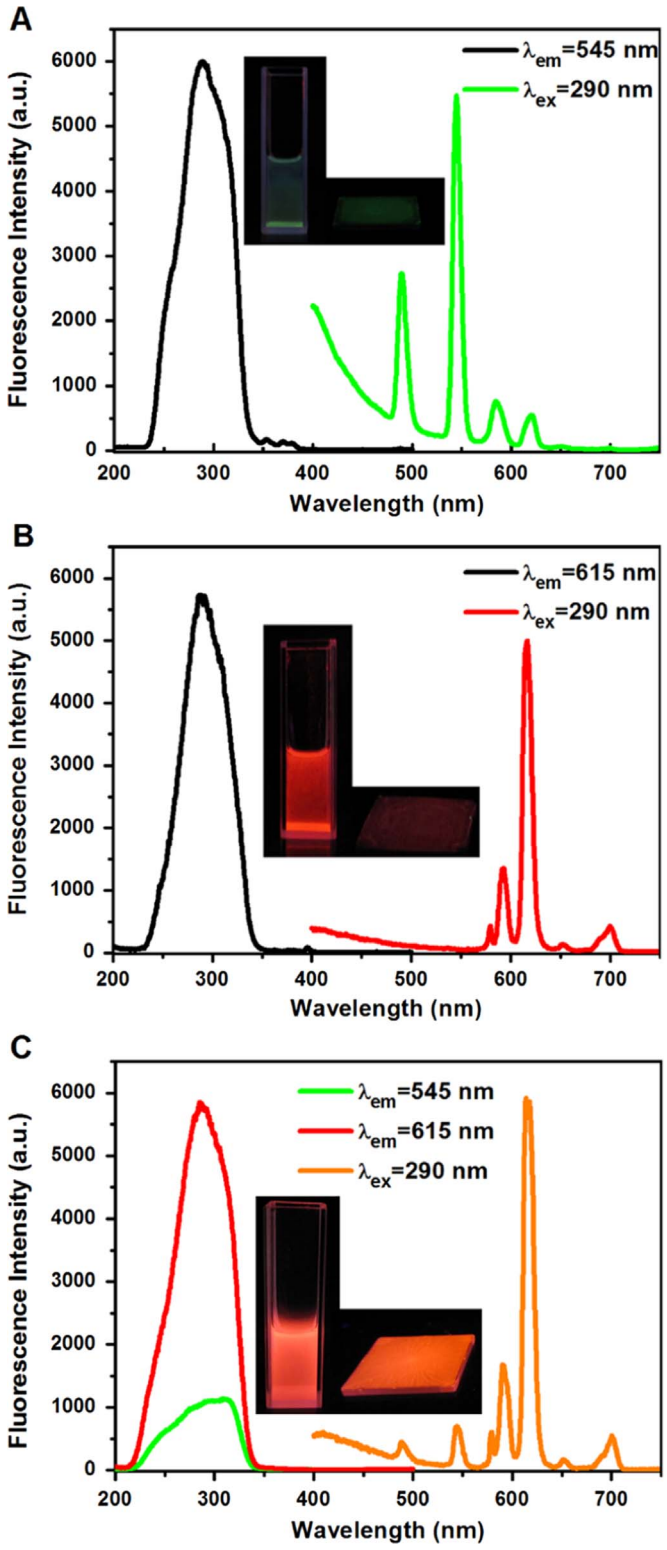

Fig. 2. The fluorescent excitation and emission spectra of (A) Tb@bio-MOF-1, (B) Eu@bio-MOF-1 and (C) Tb/Eu@bio-MOF-1. Inset: the corresponding luminescence photographs of the samples dispersed in the aqueous solution and solid films under 254 nm UV light.

488, 545, 583 and 622 nm, respectively; and Eu@bio-MOF-1 exhibits Eu^{3+} characteristic transitions at 580, 593, 615, 650 and 700 nm, respectively. When Tb/Eu@bio-MOF-1 is irradiated at 290 nm, its emission bands correspond well to both characteristic peaks of Tb^{3+} and Eu^{3+} (Fig. 2C). Its two dominant peaks at 615 nm and 593 nm are assigned to $^5D_0 \rightarrow {}^7F_J$ (J=1, 2) transitions of Eu^{3+} and the other two weaker peaks at 488 nm and 545 nm are attributed to $^5D_4 \rightarrow {}^7F_J$ (J=5, 6) transitions of Tb^{3+}. Its remaining emission peaks around 580, 650 and 700 nm are mainly from $^5D_0 \rightarrow {}^7F_J$ (J=0, 3, 4) transitions of Eu^{3+}. Even though Tb^{3+} is a dominant content in this Tb/Eu co-doping material (according to the ICP result), Eu^{3+} emission intensity is much stronger than Tb^{3+} emission. When exciting Tb/Eu@bio-MOF-1 with a common ultraviolet lamp (254 nm), it emits both Eu^{3+} and Tb^{3+} ion characteristic colors, as shown in Fig. 2(C) inset. Although H_2O molecule may quench lanthanide emission, bio-MOF-1 can sensitize and provide protection for the lanthanides.

Even Tb^{3+} is dominant in Tb/Eu@bio-MOF-1, its emission is still bright orange-red color. This interesting phenomenon may be explained by an energy transfer from Tb^{3+} to Eu^{3+} when they are immerged into bio-MOF-1 pore. To confirm this assumption, we investigate emission spectrum of Tb/Eu@bio-MOF-1 under 488 nm which is $^7F_6 \rightarrow {}^5D_4$ transition of Tb^{3+} ion. As shown in Fig. S3, emission of Eu^{3+} at 615 nm and 700 nm is detected and their fluorescence intensity is stronger than that of Tb^{3+} in this emission spectrum. This result provides a direct evidence for the energy transfer from Tb^{3+} to Eu^{3+}. In order to investigate the efficiency of energy transfer from Tb^{3+} to Eu^{3+}, emission decay curves of Tb^{3+} and Eu^{3+} ions are measured and fitted with double exponential pattern (Fig. S4). Their average lifetimes can be calculated according to Eq. (1)

$$\tau_{av}=(A_1\tau_f^2 + A_2\tau_s^2)/(A_1\tau_f + A_2\tau_s) \quad (1)$$

where τ_f and τ_s stand for the rapid process and slow process of the fluorescence lifetime, respectively. A_1 and A_2 are the pre-exponential factors of the fitted curve. Average decay times of Tb^{3+} in Tb@bio-MOF-1 and Tb/Eu@bio-MOF-1 are determined as 556.04 μs and 55.73 μs, respectively. Furthermore, the energy transfer efficiency η_T from Tb^{3+} to Eu^{3+} ions is determined using Eq. (2)

$$\eta_T=1-\tau/\tau_0 \quad (2)$$

where τ is the lifetime of Tb^{3+} in mixed lanthanide MOFs and τ_0 is the lifetime of Tb^{3+} in single lanthanide MOFs. Tb/Eu@bio-MOF-1 η_T is calculated as 89.98%, suggesting that the energy transfer is efficient. Tb^{3+}-to-Eu^{3+} energy transfer efficiency (almost 90%) in Tb/Eu@bio-MOF-1 is higher than most reported Tb^{3+}-to-Eu^{3+} energy transfer efficiency values (Jiao et al., 2013; Rao et al., 2013). Since the average decay time of Eu^{3+} is extended from 466.3 μs (Eu@bio-MOF-1) to 653.4 μs (Tb/Eu@bio-MOF-1), Eu^{3+} is considered as the energy transfer acceptor in Tb/Eu@bio-MOF-1 (Fig. S4B).

3.3. Sensing property toward DPA

DPA is an unique biomarker for *Bacillus anthracis*, we thus investigate sensing property of Tb/Eu@bio-MOF-1 towards DPA. Three different Tb/Eu molar ratios Tb/Eu@bio-MOF-1 were prepared to study the effect of Tb^{3+} ion concentration on sensor performance. DPA sensing spectra of these three samples are shown in Fig. 3. All three sensors show evident emission spectra change along with DPA addition. For the MOF with Tb^{3+}/Eu^{3+} molar ratio of 2.55 (Fig. 3A), after adding DPA, Tb^{3+}emission is gradually increased, while Eu^{3+} emission is weakened firstly and then enhanced at high DPA concentration. For the MOF with Tb^{3+}/Eu^{3+} molar ratio of 9.5 (Fig. 3B), Tb^{3+} emission is almost unchanged; while Eu^{3+} emission is weakened with the increase of DPA concentration. In the case of MOF with Tb^{3+}/Eu^{3+} molar ratio of 5.89 (Fig. 3C), with DPA addition, Tb^{3+} emission at 545 nm is gradually enhanced while Eu^{3+} emission at 615 nm is significantly

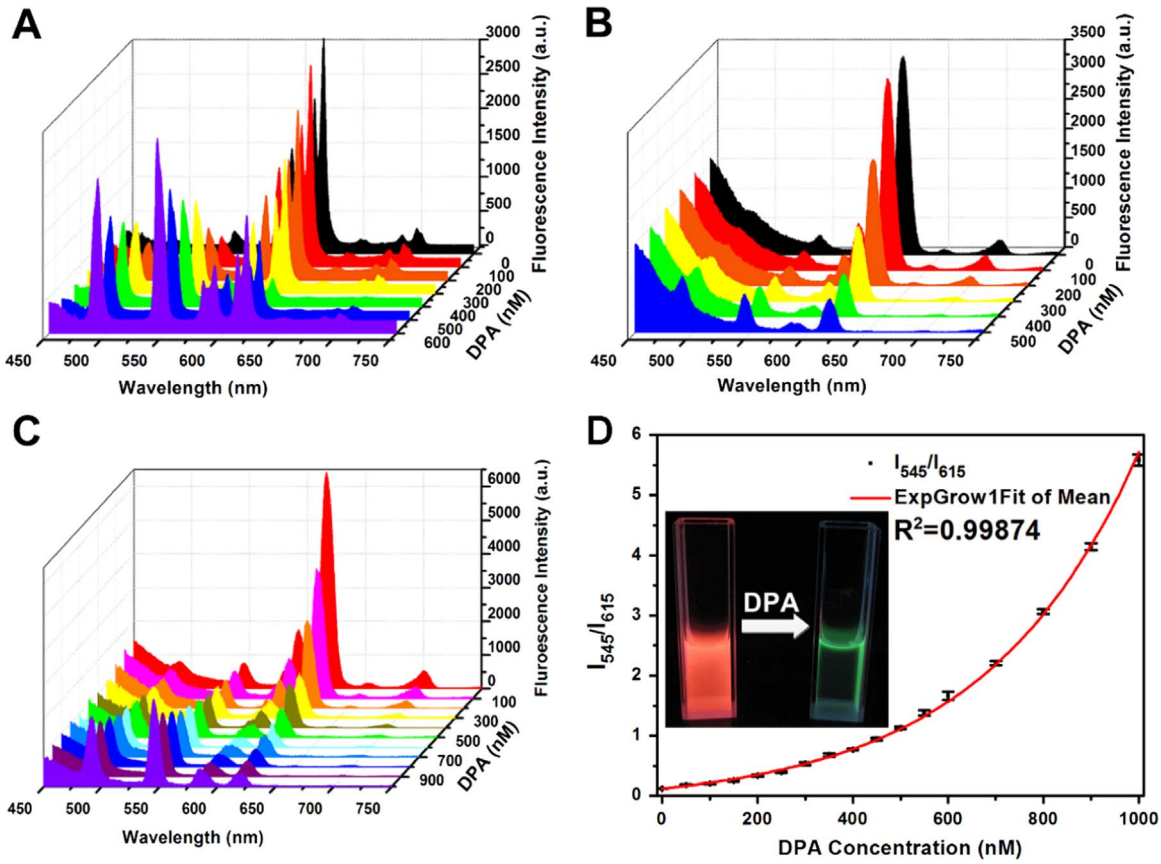

Fig. 3. DPA sensing spectra of the Tb/Eu@bio-MOF-1 with the final molar ratios of Tb^{3+}/Eu^{3+} are (A) 2.55, (B) 9.5 and (C) 5.89. (D) Plots of the relationship between the integrated intensity (I_{545}/I_{615}) of Tb/Eu@bio-MOF-1 (Tb^{3+}/Eu^{3+} =5.89) and DPA concentrations from 50 nM to 1 μM. Inset: visible color changes of Tb/Eu@bio-MOF-1 under 254 nm UV light.

weakened. More interestingly, this Tb/Eu@bio-MOF-1 with moderate Tb/Eu ratio exhibits visual colorimetric sensing: its fluorescent color changes from orange-red to green after adding different concentrations of DPA, which is recognizable with naked eyes under UV light (Fig. 3D and Fig. S5). Our following discussion of Tb/Eu@bio-MOF-1 will focus on the MOF with Tb^{3+}/Eu^{3+} molar ratio of 5.89.

The relationship between DPA concentration and fluorescence intensity of Tb/Eu@bio-MOF-1 Tb:Eu=5.89 is illustrated in Fig. 3 (D). Fluorescence intensity of each pint was measured 3 times, and corresponding average value was used to determine intensity ratio I_{545}/I_{615}. The relative standard deviations (RSD) data are listed in Table S2 in Supporting Information to make our result more convincing. When introducing different concentrations of DPA, the intensity values at 545 nm and 615 nm appear opposite change and the intensity ratio I_{545}/I_{615} increases exponentially. According to the working curve, the intensity ratio I_{545}/I_{615} is fitted well with single exponential Eq. (3).

$$I_{545}/I_{615}= 0.38514*\exp[(C_{[DPA]}- 112.35)/325.84] - 0.15395\ (R^2 = 99.87\%) \quad (3)$$

From this equation, DPA content o can be calculated quantitatively. Limit of detection (LOD) for DPA is defined as signal-to-noise (S/N) ratio=3, which is calculated as 34 nM. This value is much lower than an infectious dosage of *Bacillus anthracis* spores (60 μM) for human being (Pellegrino et al., 1998; Rosen et al., 1997). Compared to single lanthanide sensors for DPA reported by previous works (Li et al., 2013; Xu et al., 2012), these mixed lanthanide bio-MOFs need no correction, which shows a higher reliability and sensitivity. Moreover, it is easier to recognize a color change than a brightness change by naked eyes. Fig. S5 demonstrates fluorescent color change after adding DPA under a 254 nm UV lamp, where the orange-red emission becomes green after being treated with about 500 nM DPA. Therefore, Tb/Eu@bio-MOF-1 can be developed as an excellent candidate to determine DPA concentration quantitatively by intensity ratio (I_{545}/I_{615}) and qualitatively by naked eyes. In this biosensor, bio-MOF-1 acts as matrix, providing biocompatibility function and protecting lanthanides; whereas Tb^{3+} serves as a recognition element to recognize DPA, and Eu^{3+} plays a role of internal reference.

3.4. Mechanism of ratio fluorescence

In order to investigate the sensing mechanism in Tb/Eu@bio-MOF-1, emission decay dynamics data of Tb^{3+} and Eu^{3+} are compared before and after adding DPA (Fig. S6). With DPA addition, Tb^{3+} luminescence decay time in Tb/Eu@bio-MOF-1 is greatly increased while Eu^{3+} luminescence decay time is decreased, which is in agreement with their spectra change. It is observed that luminescence decay curves fit double-exponential decay well, and their average decay times are determined as 87.67 μs, 277.07 μs, 806.7 μs, 964.21 μs, and 997.05 μs with DPA concentrations ranging from 100 to 500 nM, respectively. Surprisingly, average decay times of Eu^{3+} after DPA addition are determined as 591.04 μs, 531.12 μs, 485.35 μs, 426.09 μs, and 343.43 μs, respectively, showing no obvious differences. This result demonstrates the high affinity binding of DPA to Tb^{3+} ions (Cable et al., 2009; Chen et al., 2015).

Luminescence color variation of Tb/Eu@bio-MOF-1 after DPA addition (from orange-red to green) can be explained by the transformation of energy transfer process. As depicted in

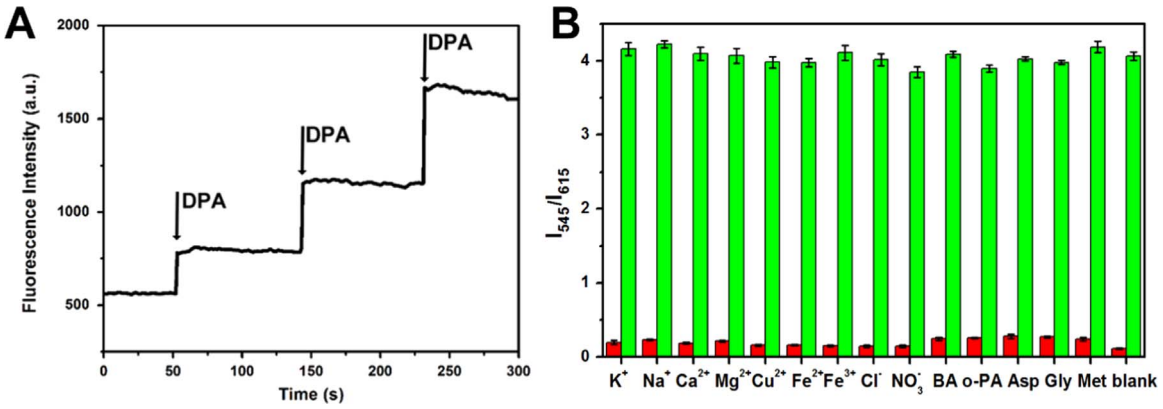

Fig. 4. (A) Fluorescence monitoring of Tb/Eu@bio-MOF-1 (545 nm) upon DPA addition in aqueous solution at room temperature (100 nM of DPA for each time). Excitation wavelength is at 290 nm. (B) Fluorescence responses of the Tb/Eu@bio-MOF-1 towards analytes including common ions, aromatic ligands, amino acids and DPA when excited at 290 nm. (n=3).

Scheme 1, before DPA addition, the energy transfer from Tb^{3+} to Eu^{3+} is dominated in Tb/Eu@bio-MOF-1, so the biosensor emits orange-red light. After adding DPA, the energy transfer from DPA to Tb^{3+} gradually becomes the dominating energy transfer process. Thus, a green emission dominates corresponding emission color. Hence, this remarkable sensing performance of Tb/Eu@bio-MOF-1 towards DPA can be ascribed to the following reasons: Firstly, DPA chelates with Tb^{3+} ions and forms ligand-to-metal energy transfer. Secondly, the reversible energy transfer tendency between Tb^{3+} and Eu^{3+} enhances their response signal.

3.5. Time response and selectivity of Tb/Eu@bio-MOF-1 sensors

Response time is significant for biosensors, since biological threat may be more damaging as time goes on. Time-dependent fluorescence intensity curve was taken by monitoring the emission at 545 nm under 290 nm excitation. As shown in Fig. 4**A**, luminescence intensity of Tb^{3+} in Tb/Eu@bio-MOF-1 is very weak but stable in its initial period. After adding DPA (100 nM) into Tb/Eu@bio-MOF-1 solutions (0.25 mg mL^{-1}), the curve shows a rapid ascent in the first 10 s and becomes constant after 20 s This result demonstrates that Tb/Eu@bio-MOF-1 sensor can work in fast, continuous and on-line monitoring of DPA.

Selectivity is another important parameter for chemical sensors. Hence, we investigated fluorescence response of Tb/Eu@bio-MOF-1 towards other potentially interfering aromatic ligands and representative amino acids including benzoic acid (BA), o-phthalic acid ((*o*-PA)), and 1,3,5-benzenecarboxylic acid (BTC), as well as D-aspartic (Asp), glycine (Gly) and methionine (Met). These compounds are either structurally related to DPA or potentially existed in biological environments, which contain carboxylic acid groups and may coordinate with Tb^{3+} ions. In addition, common cellular ions such as K^+, Na^+, Ca^{2+}, Mg^{2+}, Cu^{2+}, Fe^{2+}, Fe^{3+}, Cl^- and NO_3^- are selected as the co-exist with DPA in the bacterial spores and animals and to research their effect on Tb/Eu@bio-MOF-1. All samples are tested under identical condition with their fluorescent response illustrated in Fig. 4(B). Remarkably, even the concentration of interfering groups is twice of DPA, slight or negligible fluorescence change is observed. Only DPA can lead to a prominent fluorescence change, which indicates that Tb/Eu@bio-MOF-1 has a good selectivity for detection of *anthrax* biomarker DPA.

3.6. Detection of DPA in human serum

To explore performance of Tb/Eu@bio-MOF-1 towards DPA in real physiological environment, different levels of standard DPA concentrated solution were added in undiluted serum samples and then measured. By converting the luminescence intensity ratio to concentration through above characteristic Eq. (3), DPA concentrations in human serum can be estimated with their result displayed in Table 1. DPA recovery values in human serum samples are between 97.85% and 106.35% and the relative standard deviation (RSD, n=3) are all $<1.18\%$. The almost no influence caused by bio-molecules in serum such as phospholipid may be attributed to the nano-pore size selectivity of bio-MOF-1. In spite of the small error, Tb/Eu@bio-MOF-1 can be one of potential candidates which are used for detecting DPA in serum samples.

Table 1
Determination of DPA in human serum samples.

Added (10^{-7} M)	Founded (10^{-7} M)	Recovery (%)	RSD (n=3) (%)
2.0	2.06 ± 0.018	102.85	0.90
3.0	3.19 ± 0.011	106.35	1.18
4.0	3.91 ± 0.035	97.85	0.28

4. Conclusion

In conclusion, using biocompatible and porous MOFs as matrix and protector, using Tb^{3+} as response unit, and co-doping Eu^{3+} as an internal reference, we presented a facile, rapid, highly sensitive and selective strategy for the ratiometric fluorescent detection of a bacillus spores biomarker. The Tb^{3+}/Eu^{3+} functionalized bio-MOF-1 was easily prepared by cation exchange process. As a ratiometric fluorescent sensor, Tb^{3+} emission was enhanced by DPA through ligand-to-metal energy transfer and Eu^{3+} emission was quenched due to the interruption of energy transfer from Tb^{3+} to Eu^{3+}, which gave Tb/Eu@bio-MOF-1 sensor high sensitivity and excellent selectivity sensing performance for DPA. This sensor showed a good single exponential response for DPA with a detection limit of 34 nM, which was much lower than an infectious dosage of the *Bacillus anthracis* spores (60 μM) for human being. Importantly, Tb/Eu@bio-MOF-1 emission color was changed from orange-red to green after introducing DPA, which was recognizable with naked eyes under UV light. By regulating the energy transfer process in Tb/Eu@bio-MOF-1, we realized visual colorimetric sensing of DPA in porous MOFs for the first time. The excellent sensing performance of Tb/Eu@bio-MOF-1 in human serum demonstrated that this sensor was reliable and practical in practical applications. We believe that this ratiometric Tb/Eu@bio-

MOF-1 sensor can provide a new method for conveniently and rapidly detection of bacterial spores.

Acknowledgements

The authors gratefully thank the financial supports of the NSFC (Grant Nos. 51372240, 51572256, 21501166).

Appendix A. Supplementary material

Supplementary data associated with this article can be found in the online version at http://dx.doi.org/10.1016/j.bios.2016.05.020.

References

Ai, K., Zhang, B., Lu, L., 2009. Angew. Chem. Int. Ed. 48 (2), 304–308.
An, J., Geib, S.J., Rosi, N.L., 2009. J. Am. Chem. Soc. 131 (24), 8376–8377.
An, J., Shade, C.M., Chengelis-Czegan, D.A., Petoud, S., Rosi, N.L., 2011. J. Am. Chem. Soc. 133 (5), 1220–1223.
Cable, M.L., Kirby, J.P., Levine, D.J., Manary, M.J., Gray, H.B., Ponce, A., 2009. J. Am. Chem. Soc. 131 (27), 9562–9570.
Chen, B., Xiang, S., Qian, G., 2010. Acc. Chem. Res. 43 (8), 1115–1124.
Chen, H., Xie, Y., Kirillov, A.M., Liu, L., Yu, M., Liu, W., Tang, Y., 2015. Chem. Commun. 51 (24), 5036–5039.
Das, R., Goel, A.K., Sharma, M.K., Upadhyay, S., 2015. Biosens. Bioelectron. 74, 939–946.
Eliseeva, S.V., Bunzli, J.C., 2010. Chem. Soc. Rev. 39 (1), 189–227.
Gao, R., Ko, J., Cha, K., Jeon, J.H., Rhie, G.E., Choi, J., deMello, A.J., Choo, J., 2015. Biosens. Bioelectron. 72, 230–236.
Guan, Y., Qu, S., Li, B., Zhang, L., Ma, H., Zhang, L., 2015. Biosens. Bioelectron. 77, 124–130.
Hurtle, W., Bode, E., Kulesh, D.A., Kaplan, R.S., Garrison, J., Bridge, D., House, M., Frye, M.S., Loveless, B., Norwood, D., 2004. J. Clin. Microbiol. 42 (1), 179–185.
Jiao, M., Guo, N., Lu, W., Jia, Y., Lv, W., Zhao, Q., Shao, B., You, H., 2013. Dalton Trans. 42 (34), 12395–12402.
Lepage, D., Jiménez, A., Beauvais, J., Dubowski, J.J., 2013. Light Sci. Appl. 2 (4), e62.
Li, B., Zhang, Y., Ma, D., Ma, T., Shi, Z., Ma, S., 2014. J. Am. Chem. Soc. 136 (4), 1202–1205.
Li, G., Hou, Z., Peng, C., Wang, W., Cheng, Z., Li, C., Lian, H., Lin, J., 2010. Adv. Funct. Mater. 20 (20), 3446–3456.
Li, Q., Sun, K., Chang, K., Yu, J., Chiu, D.T., Wu, C., Qin, W., 2013. Anal. Chem. 85 (19), 9087–9091.
Oh, W.K., Jeong, Y.S., Song, J., Jang, J., 2011. Biosens. Bioelectron. 29 (1), 172–177.
Pellegrino, P.M., Fell, N.F., Rosen, D.L., Gillespie, J.B., 1998. Anal. Chem. 70 (9), 1755–1760.
Rao, X., Song, T., Gao, J., Cui, Y., Yang, Y., Wu, C., Chen, B., Qian, G., 2013. J. Am. Chem. Soc. 135 (41), 15559–15564.
Rosen, D.L., Sharpless, C., McGown, L.B., 1997. Anal. Chem. 69 (6), 1082–1085.
Shen, X., Yan, B., 2015a. J. Colloid Interface Sci. 451, 63–68.
Shen, X., Yan, B., 2015b. Dalton Trans. 44 (4), 1875–1881.
Su, J., Goldberg, A.F.G., Stoltz, B.M., 2016. Light Sci. Appl. 5 (1), e16001.
Tsukube, H., Shinoda, S., 2002. Chem. Rev. 102 (6), 2389–2404.
Wang, Y., Li, B., Zhang, L., Li, P., Wang, L., Zhang, J., 2012. Langmuir 28 (2), 1657–1662.
Webb, G.F., 2003. Proc. Natl. Acad. Sci. 100 (8), 4355–4356.
White, K.A., Chengelis, D.A., Zeller, M., Geib, S.J., Szakos, J., Petoud, S., Rosi, N.L., 2009. Chem. Commun. 30, 4506–4508.
Xu, H., Rao, X., Gao, J., Yu, J., Wang, Z., Dou, Z., Cui, Y., Yang, Y., Chen, B., Qian, G., 2012. Chem. Commun. 48 (59), 7377–7379.
Yilmaz, M.D., Hsu, S.H., Reinhoudt, D.N., Velders, A.H., Huskens, J., 2010. Angew. Chem. Int. Ed. 49 (34), 5938–5941.
Yu, D.C., Martín-Rodríguez, R., Zhang, Q.Y., Meijerink, A., Rabouw, F.T., 2015. Light Sci. Appl. 4 (10), e344.
Yung, P.T., Lester, E.D., Bearman, G., Ponce, A., 2007. Biotechnol. Bioeng. 98 (4), 864–871.
Zhang, J., Hao, Z., Li, J., Zhang, X., Luo, Y., Pan, G., 2015. Light Sci. Appl. 4 (1), e239.
Zhang, X., Young, M.A., Lyandres, O., Van Duyne, R.P., 2005. J. Am. Chem. Soc. 127 (12), 4484–4489.
Zhao, S.N., Li, L.J., Song, X.Z., Zhu, M., Hao, Z.M., Meng, X., Wu, L.L., Feng, J., Song, S.Y., Wang, C., Zhang, H.J., 2015. Adv. Funct. Mater. 25 (9), 1463–1469.
Zou, J., Peng, Y.-G., Tang, Y.-Y., 2014. RSC Adv. 4 (19), 9693–9700.